

Formability and FEM Simulation of Steel Sheets in the Hot Stamping Process

Kazuhisa KUSUMI*
Jun MAKI

Naruhiko NOMURA

Abstract

Production of parts by means of hot stamping process has increased. Applications of hot stamping contribute to the weight reduction of automobiles by the production of parts with both high strength and excellent shape fixability. In this report, basic formability and FEM analysis of hot stamping were presented. In addition, the corrosion resistance of hot stamped aluminized steels was discussed.

1. Introduction

In recent years, the application of hot-stamped auto parts as a means of reducing automobile weight has been expanding. **Fig. 1** illustrates schematically the hot stamping process, in which the steel sheet is first heated to an austenitic temperature (A_{c3} or higher). It is then taken out of the furnace and transferred to the press machine, where it is formed and quenched by water-cooled dies.¹⁾ Boron steels with added elements, e.g., Mn and B, are used as materials for hot stamping.²⁾ The typical chemical composition of boron steel sheet is shown in **Table 1**. Using this steel sheet, it is possible to hot stamp auto parts with a tensile strength of about 1,500 MPa. A major advantage of hot stamping is that it offers excellent shape fixability of the stamped steel sheet, whereas the poor shape fixability of ultrahigh-strength steel sheet subjected to cold stamping is a major drawback. Hot stamping permits the manufacture of auto parts with high strength and excellent shape accuracy.

To investigate the formability of steel sheet under high tempera-

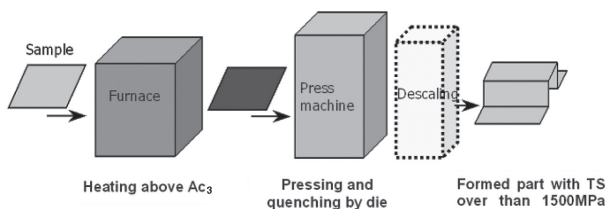


Fig. 1 Schematic diagram of hot stamping process

Table 1 Chemical compositions of hot stamped steel sheet²⁾

C	Mn	Cr	B
0.22	1.2	0.2	0.002

tures, studies on formability have been conducted in warm forming using heated tools.^{3,4)} However, limited information is available regarding the press formability of steel sheet in hot stamping utilizing higher temperatures and cold tools. Therefore, we studied basic characteristics of press formability and developed an FEM simulation technique for hot stamping coupling heat treatment and plastic deformation to study the formability of actual automotive parts of complicated shapes. In addition, we discussed the corrosion resistance of hot-stamped parts of aluminized steel sheet.

2. Formability of Steel Sheet in Hot Stamping

2.1 Shape fixability in bending work^{5,6)}

When a steel sheet is formed, it exhibits an elastic recovery corresponding to the forming force applied. Therefore, the amount of elastic recovery increases when a higher strength steel sheet is formed, causing its springback to increase and its shape fixability to decrease. By applying hot stamping, however, it is possible to obtain parts with high strength and good shape fixability. Therefore, we initially compared the differences in shape fixability between hot stamping and cold stamping for various steel sheets of different strength. **Fig. 2** illustrates the appearances of stamped steel sheets, and **Fig. 3** shows the relationship between the amount of springback

* Manager, Research Planning Dept., Steel Research Laboratories
20-1 Shintomi, Futtsu, Chiba 293-8511

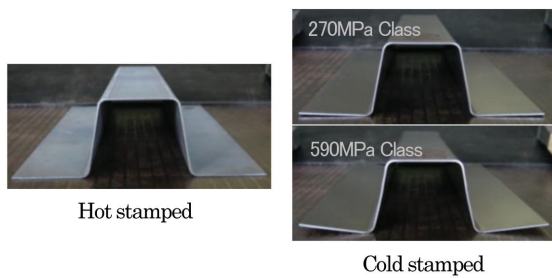


Fig. 2 Comparison of shape fixability between cold and hot stamped parts

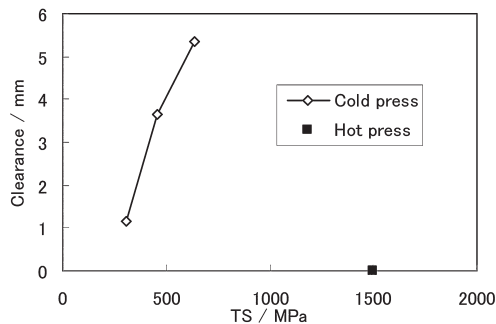


Fig. 3 Relation between spring-back and tensile stress of steel sheet

and the strength of the steel sheet. For cold stamping, the amount of springback increases with increasing sheet strength. Conversely, the springback in hot stamping is almost zero. Thus, it has been found that shape fixability is much better for hot stamping than for cold stamping.

It should be noted, however, that a forming force occurs even in hot stamping and that the steel sheet might be subject to corresponding springback. Furthermore, the steel sheet in hot stamping undergoes martensite transformation while being held at the bottom dead point after the press forming. This process may affect the stress introduced into the steel sheet during the forming process. Therefore, we have chosen to study the influence of martensite transformation on shape fixability.

We used a specimen of aluminized steel sheet for hot stamping (0.2%C steel in Table 2 and Fig. 4). As reference steels, we used 270 MPa IF steel (hereinafter referred to as IF steel) and SUS 304, both of which exhibit a transformation behavior different from that of 0.2%C steel. After the three steel sheets were heated to 950°C, they were air cooled and the forming start temperature was varied between 400°C and 800°C. When air cooled to 550°C or lower, the steel sheet for hot stamping transformed into bainite; the sheet was austenite at the forming start temperatures in the range 600°C to 800°C and transformed to martensite while being held at the bottom dead point after forming. When the forming start temperature was 500°C or lower, the steel sheet transformed to bainite before forming; hence, martensite transformation did not occur while the sheet was held at the bottom dead point after forming. Conversely, the IF steel and SUS 304 were ferrite and austenite, respectively, for the abovementioned temperature range, and neither of these steels underwent any transformation during forming or while being held at the bottom dead point on the press. The phases of the three types of steel in the forming temperature range are shown in Table 2.

Fig. 4 shows the influence of forming temperature on shape fix-

Table 2 Phases of the each type of steels at the forming start temperature

Forming temperature (°C)	0.2%C steel	IF steel	SUS304
800	γ	α	γ
700	γ	α	γ
600	γ	α	γ
550	γ	—	—
500	B	α	γ
450	B	—	—
400	B	α	γ

γ : austenite α : ferrite B: bainite

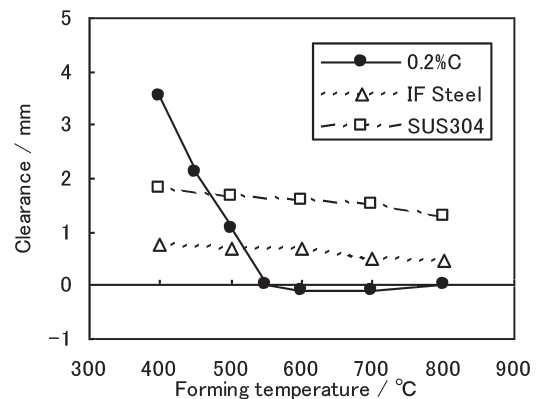


Fig. 4 Dependence of shape fixability on forming temperature

ability of each type of steel. The steel sheet for hot stamping showed good shape fixability when the forming temperature was as high as 550°C to 800°C, and martensite transformation took place after forming. However, when the forming temperature was below 500°C, the temperature at which bainite transformation began, the shape fixability of the steel sheet deteriorated sharply. Furthermore, the IF steel and SUS 304, which were free from any transformation, exhibited springback even when the forming temperature was 800°C. Their shape fixability deteriorated continuously with the decline in the forming temperature, which we attribute to the increase in deformation resistance as the forming temperature was lowered. In the case of the steel sheet for hot stamping, the amount of springback was very small at a high forming temperature, where martensite transformation took place after forming. However, the steel sheet exhibited considerable springback for a forming temperature beyond bainite transformation, indicating that its shape fixability is influenced more or less by martensite transformation.

Fig. 5 illustrates the relationship between shape fixability and hot tensile strength. For the IF steel and SUS 304 (which are free from martensite transformation after forming) and the steel sheet for hot stamping formed at 400°C, there is a linear relationship between shape fixability and hot tensile strength. Conversely, the steel sheet for hot stamping that was formed in the austenite region (at 600°C, 700°C, and 800°C) and underwent martensite transformation after forming exhibited very low shape fixability regardless of its hot tensile strength. The above observations suggest that, when martensite transformation takes place after forming, the steel sheet for stamping displays good shape fixability regardless of its hot tensile strength.

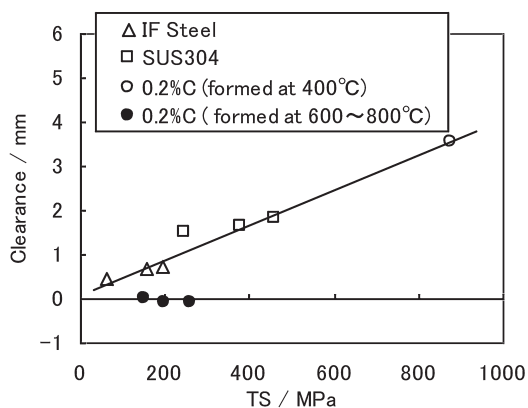


Fig. 5 Dependence of shape fixability on hot tensile strength

From the above results, we concluded that the steel sheet displays excellent shape fixability when it undergoes martensite transformation after forming, which we explain as follows. A stress corresponding to deformation resistance is introduced into the steel sheet during forming. Subsequently, if martensite transformation does not take place, the stress that has been introduced into the steel sheet during forming remains there even after cooling. The stress is relieved only after the steel sheet is removed from the press, causing springback. Conversely, if martensite transformation takes place after forming, the stress introduced into the steel sheet during forming is reduced by martensite transformation, causing the amount of springback to decrease markedly. A transformation plasticity that occurs in the direction in which the stress is relieved during the transformation has been considered as the mechanism whereby martensite transformation relieves the stress.^{7,8)}

2.2 Stretch formability⁹⁾

Fig. 6 shows the limiting dome heights for several different steel sheets in a spherical stretch forming test. The tools used in the test included a punch (R = 50 mm) and dies (R = 20 mm and 5 mm). Here hot stamping exhibited a forming limit comparable to that of 270-440 MPa steels in cold stamping and much higher than that of 1,470 MPa steel in cold stamping.

Fig. 7 shows the thickness and cross-sectional hardness distributions in the hot-stamped samples in which necking occurred. The flanges and the part at the center of the punch had been hardened to about HV 400 to 500. Conversely, the hardness of the other parts of the steel sheet, which were considered to have been out of contact with the tools, had decreased. In general, such a decrease in hardness can be avoided since the dies are designed such that they make contact with the entire surface of the steel sheet being formed. With the increase in distance from the center of the punch, the steel sheet gradually decreased in thickness and displayed its smallest thickness in the vicinity of the part where the steel sheet separated from the tool.

Fig. 8 compares the thickness distribution of cold-stamped and hot-stamped steel sheets. We found that the decrease in sheet thickness at the part in contact with the punch was less conspicuous in hot stamping than in cold stamping, and that the strain in the steel sheet was comparatively uneven, concentrated in the fracture-sensitive part.

The part of the steel sheet at the center of the punch and the flanges (which we consider to have been subjected to sufficient surface pressure through contact with the tool) exhibit appreciable

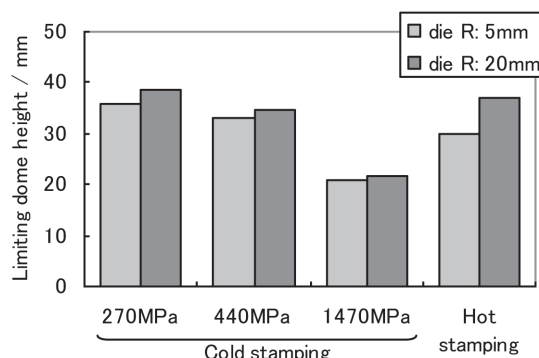


Fig. 6 Comparison of limiting dome heights by hot and cold stamping

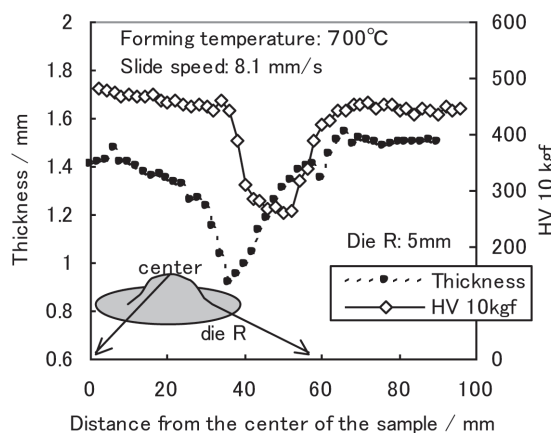


Fig. 7 Distribution of thickness and hardness of hot stamped parts

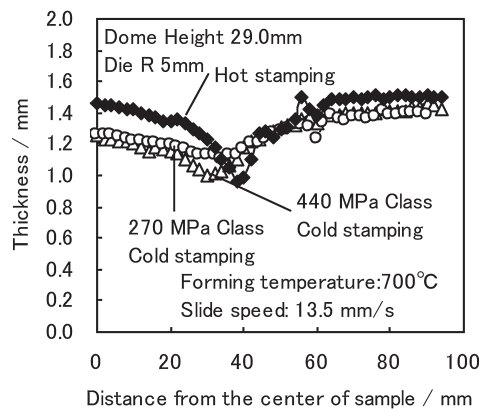


Fig. 8 Comparison of thickness distributions by hot and cold stamping

quench hardness. We believe that these parts were subjected to a considerable decline in temperature during forming because of the transfer of heat to the dies; hence, the sheet deformation resistance increased significantly. Conversely, for the parts not in contact with the tool, the transfer of heat was achieved by air cooling in the thickness direction and at the surface of the steel sheet. Therefore, it is believed that the decline in temperature during forming and the deformation resistance of these parts are smaller than those of the parts in contact with the tool. As a result, the deformation of the

steel sheet concentrates in the highly strained part around the center of the punch, where the tool does not make contact with the sheet. This is considered to cause necking in the part indicated in Fig. 7, eventually causing fracturing.

In ordinary stretch forming, the uniformity of deformation of the material is influenced by the shape of the tool (part), the coefficient of friction between the tool and the material, and the n-value (work hardening coefficient) of the material. In hot stamping, a change in the temperature of the material caused by the transfer of heat through contact with the tool results in uneven material properties. This is also considered to influence the uniformity of deformation of the material and govern the forming limit.

2.3 Draw bending formability¹⁰⁾

We studied the forming limit in draw bending, in which the flanges are free from deformation, as a basic investigation of the deep drawability of steel sheet. Here strip specimens were used, each measuring 1.4 mm × 100 mm × 400 mm, and the influences of forming speed and blank holding force on forming limit were studied using the draw bending tool illustrated in Fig. 9.

Fig. 10 shows the appearance of a fractured part; it can be seen that the fracture occurred in the part between the punch shoulder R and the die shoulder R. The mode of fracture was always as shown in the Fig. 2, regardless of the forming conditions.

Fig. 11 shows the effects of forming height, forming speed, and blank holding force on draw bendability under a forming start temperature of 800°C and blank holding forces of 2.3, 3.7, and 5.7 tonf. It can be seen from the figure that a fracture tends to occur easily when values of both forming speed and blank holding force are high.

Fig. 12 shows the relationship between critical forming speed and critical blank holding force in terms of fracture, derived from the above results and the results of a test using a forming start temperature of 700°C. The low-speed side under each of the two straight lines represents the formable region. It is clear from the figure that the smaller the blank holding force, the lower the forming start temperature; additionally, the lower the forming speed, the better the draw bendability in hot stamping.

It is assumed that the fracture-sensitive part that does not make contact with the tool increases in temperature and decreases in deformation resistance during draw forming. Conversely, when the

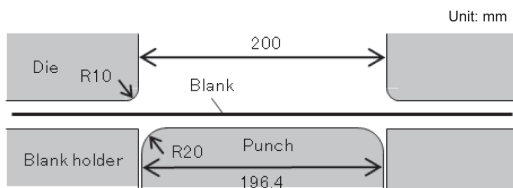


Fig. 9 Cross-sectional profiles of tool

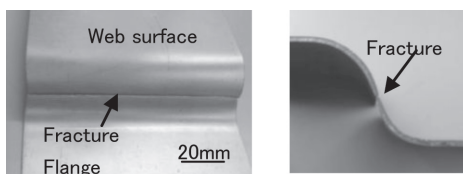


Fig. 10 Aspects of fracture part (formed under a temperature of 800°C, at a rate of 12.7mm/s, with a blank holder force of 2.3 tonf and to a height of 30mm)

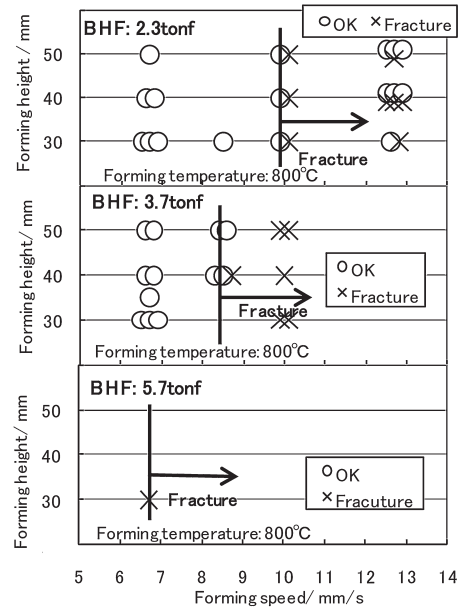


Fig. 11 Effects of forming heights, forming speeds and blank holder forces affecting formability (under a temperature of 800°C at the start of forming)

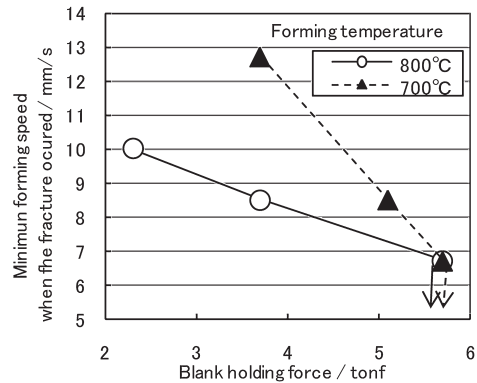


Fig. 12 Relation between minimum forming speeds and blank holder forces when fracture occurred

forming speed and forming start temperature are low, it is assumed that the fracture-sensitive part between the punch shoulder and die shoulder increases in terms of deformation resistance and becomes less sensitive to fractures. Thus, the temperature at the center of the side wall in the early stages of forming was assumed to be the factor governing draw bendability in hot stamping.

2.4 Corrosion resistance of hot-stamped aluminized steel sheet

It has been reported that the corrosion resistance of hot-stamped aluminized steel sheet (coating weight: 160 g/m² both side) is comparable to that of an ordinary rust-preventive steel sheet—galvannealed (GA) steel sheet or galvanized (GI) steel sheet.^{2, 11, 12)} It has also been reported that aluminized steel sheet displays a laminar structure, as shown in Fig. 13, when it is heated in a hot stamping process.¹²⁾ Let us name the five layers a, b, c, d, and e from top to down. Layers a and c contain about 50% Al, which is estimated to consist mainly of Fe₂Al₃. Conversely, layers b and d contain about 30% Al and are of Fe-rich phase. Layer e, which is nearest to the steel sheet, is of α-Fe phase and contains 10% or less Al in the form

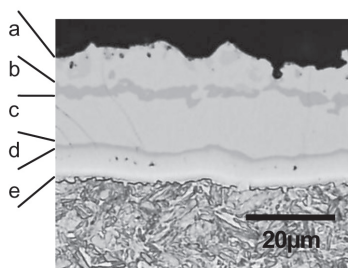


Fig. 13 Cross-section of the surface layer after holding at 900 °C for 2 minutes

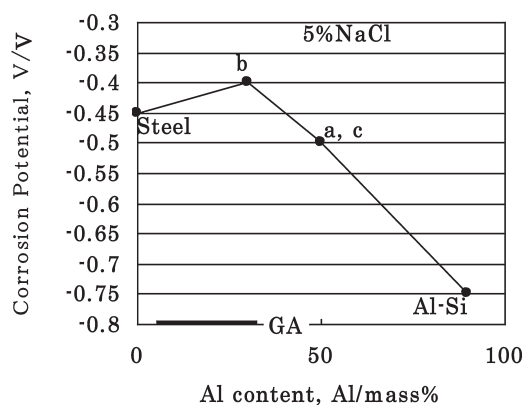


Fig. 14 Influence of Al content on the corrosion potential of materials in the 5% NaCl solution

of solid solution.

The corrosion potential of each of layers a-e in 5% NaCl solution has been measured with the aim of characterizing the corrosion behavior of the above steel material.¹¹⁾ The solution used for measurement was adjusted to pH7 and a saturated calomel electrode was used as a reference electrode. For comparison, aluminized steel sheet, cold-rolled steel sheet, and GA sheet were also measured. The results of measurement of corrosion potential relative to Al concentration are shown in Fig. 14. In the corrosive environment, layers a and c display a less noble potential than the steel sheet, whereas layer b has a slightly nobler potential than the steel sheet. However, all three of these layers (a-c) display a potential nobler than that of Al-Si. Except for layer b, the corrosion potential of the layers is proportional to the Al concentration: the higher the Al concentration of a layer, the closer its potential is to that of Al. On the basis of these measurements of corrosion potential, it is assumed that layers a and c exhibit a less noble potential than layer b and corrode preferentially.

As shown in Fig. 14, the materials under consideration have a less noble potential than the steel sheet in the corrosive environment. However, since the potential difference between them is small compared to that between Zn-coated materials, it is necessary to confirm corrosion resistance when the plating is scratched or cracked. Using hat-shaped parts such as those shown in Fig. 2, we evaluated the corrosion resistance of the vertical walls and horizontal flanges. The ordinary phosphate coating and cathodic paint processes for automobiles were applied under standard conditions. The target cathodic paint thickness was 20 μm. Each specimen whose paint was scratched was subjected to 150 cycles (50 days) of

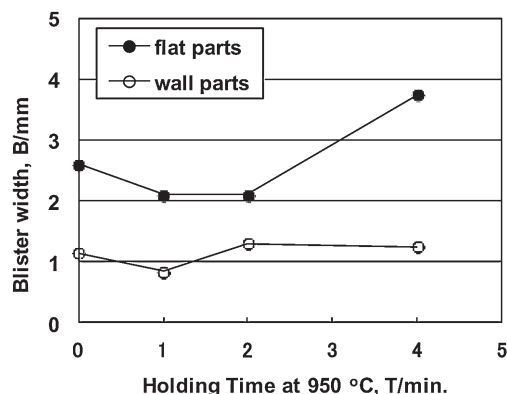


Fig. 15 Comparison of blister width between flat parts and wall parts

JASO-CCT tests (JASO-M610-92), and the width of the paint blister and depth of the steel substrate's corrosion after the test were measured.

The heating temperature was 950°C and the holding time was varied from 0 min (the specimen was cooled down immediately after reaching 950°C) to 4 min. The measurements of the paint blister width after the JASO-CCT test are shown in Fig. 15. For the flat flanges that were formed to a small degree, the blister became wider for longer holding times. Conversely, the blister width of the paint on the vertical walls was small overall, about half that on the flat parts. Under all test conditions, the depth of corrosion of the steel substrate was smaller than that of GA.

Observation of the walls of formed parts revealed cracks in the plating layer. However, a layer of phosphate coating had formed at the root of these cracks. A similar (but partial) layer of phosphate coating was also observed on the wall surfaces. It has previously been assumed that an alloyed Al-Fe surface such as that on steel sheet for hot stamping would be free from deposition of phosphate crystal:²⁾ although the phosphating reaction requires etching by the phosphating solution, the oxide film formed on the Al-Fe surface is barely etched by such a solution.

It is estimated that, on the walls and other parts that were subjected to a strong sliding force, the oxide film formed and was destroyed and the phosphating crystal formed locally. It has been shown that the coating adhesion of ordinary zinc-coated steel sheet improves markedly as a phosphate coating is formed and that the phosphate coating acts as a pH buffer in the corrosion of the substrate beneath the paint.¹³⁾ A similar process is thought to occur on the Al-Fe surface, effectively enhancing the rust-preventive effect of the coating. Namely, although cracks occur in the plating on formed parts, the rust-preventive effect of phosphate coating is thought to more than offset the corroding effect of the cracks, thereby improving the corrosion resistance of the formed parts. In this subsection, the corrosion resistance of aluminized steel sheet has been discussed. Recently, the application of Zn-coated steel sheet with good corrosion resistance has also been increasing.

3. FEM Simulation of Hot Stamping

3.1 Necessity of FEM simulation for hot stamping process

During the hot stamping process, the steel sheet is first heated to 900°C or over and then formed while still hot (at temperatures around 800°C). Subsequently, the steel sheet is cooled rapidly by dies at 150°C or lower to increase its strength by hardening. During

forming, a marked temperature difference occurs between the part of the steel sheet in contact with the dies and the part not making contact, changing the strength of the steel sheet. As a result, the formability of steel sheet changes in a complicated manner according to, forming temperature in hot stamping (unlike in cold stamping). Therefore, in order to understand the conditions of steel sheet forming and predict the formability of steel sheet on actual parts of complex shape, it is essential to analyze forming coupled with thermal effect. Recently, such a structural-thermal coupled FEM simulation was incorporated into a general structural FEM program developed for press forming. However, owing to the difficulty involved in measuring high-temperature properties and grasping the conditions of forming, there are problems yet to be solved in terms of setting analysis conditions and evaluating analysis results. Therefore, Nippon Steel Corporation is pressing ahead with the development of new simulation methods mainly by LS-DYNA.

3.2 Identifying parameters for thermal calculations

The values of high-temperature mechanical properties and friction and heat transfer coefficients necessary for structural-thermal coupled analysis were obtained by experimentation.

3.2.1 Mechanical properties at high temperatures

High-temperature stress-strain curves were defined on the basis of the results of a high-temperature strength test of aluminized steel sheet for hot stamping, taking into account temperature and strain rate, as shown in Fig. 16.

3.2.2 Friction coefficient

Ordinarily, in hot stamping lubrication was not used; therefore, the friction coefficient applicable in the forming process is estimated to be high. Nevertheless, little information exists about the friction coefficient applicable in high-temperature regions. Therefore, hot test pieces were subjected to a drawing test machine for cold sheets, as shown in Fig. 17, to determine the appropriate friction coefficient. The friction coefficient to be used in the FEM simulation was determined to be 0.5 to 0.6 on the basis of the test results. This value

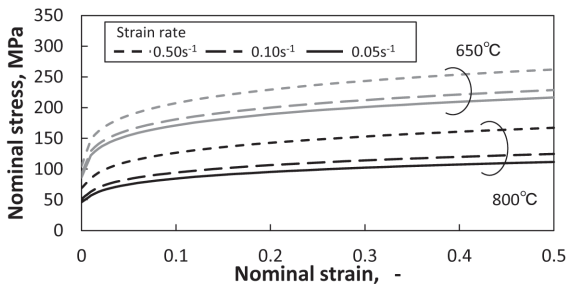


Fig. 16 Basic pattern of stress-strain curve at high temperature

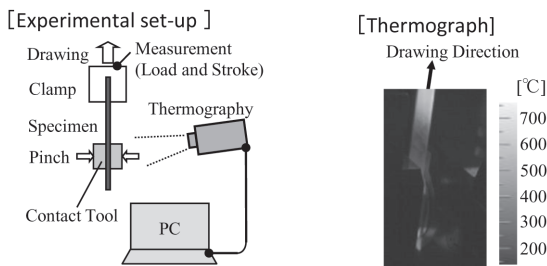


Fig. 17 Measurement of friction coefficient by drawing test on high temperature

is comparable to that presented in a recent report.¹⁴⁾

3.2.3 Heat transfer coefficient

The heat transfer coefficients most appropriate to the boundary conditions for the FEM simulation were determined using the experimental setup for hot stamping and thermal measurement shown in Fig. 18. Another die configuration for forming was tested in addition to the configuration for deep drawing shown. Thermographs obtained are shown in Fig. 19. The temperature changes were analyzed and heat transfer coefficients at the individual parts of the dies were calculated on the basis of the thermographs obtained before and after hot stamping. Fig. 20 shows the results of heat transfer coefficients for both drawing and forming. In drawing, the shoulder R and emboss in strong contact with the dies exhibit a high heat transfer coefficient; in forming, however, the calculated heat transfer coefficients are somewhat lower because there are many noncontact processes and the temperature changes are small. It should be noted

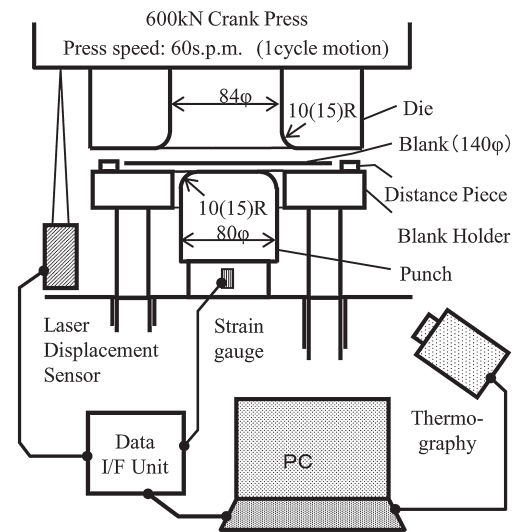


Fig. 18 Experimental set-up for hot stamping and thermal measurement

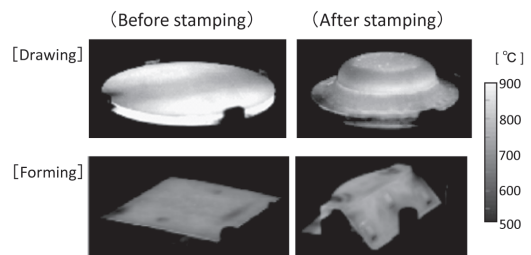


Fig. 19 Temperature distribution before and after hot stamping

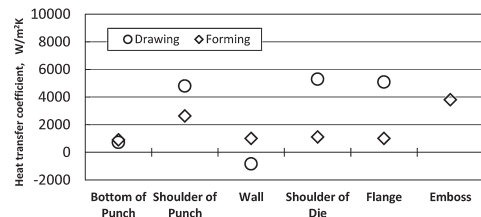


Fig. 20 Heat transfer coefficients between surfaces of blank and tool calculated from temperature histories

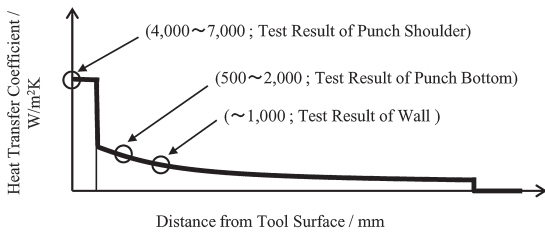


Fig. 21 Boundary condition for heat transfer defined by experimental results

that the negative value for the wall in drawing is due to the influence of the heat generated by plastic work in the portion of a fracture. In both drawing and forming in our test, the temperature region was roughly divided into contacting and noncontacting areas. Therefore, the heat transfer coefficient in the FEM simulation was given as a function of distance between the contact faces, as shown in Fig. 21.

3.3 Simulation model

A structural-thermal coupled simulation corresponding to the above test was carried out using the structural FEM program LS-DYNA (Ver. 971). The model configuration is shown in Fig. 22. Elastic-plastic shell elements were used to represent the blank and rigid shell elements to represent the tools. The blank element size was approximately 2 mm. In accordance with the measurement results, the initial blank temperature was set in the range 700°C to 850°C and the initial die temperature was set at 80°C. The conditions of heat transfer were reproduced by defining a heat capacity based on a virtual thickness defined for the tools.

The influence of element size on the accuracy of judgment of heat transfer (contact) at curved surfaces may be considered a problem in the performance of the necessary calculations. As shown in Fig. 23, the smaller the element size, the higher the accuracy of temperature calculation. Naturally, however, subdividing the element increases calculation time significantly.

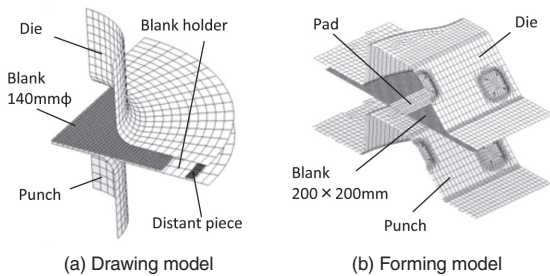


Fig. 22 Simulation models for hot stamping

Mesh size: 2mm	Mesh size: 1mm	Mesh size: 0.5mm
CPU time 2.5Hr	CPU time 20Hr	CPU time 7days

*Target temperature by tests: 730°C on shoulder of punch

Fig. 23 Influence on accuracy of thermal calculation with mesh size of simulation model

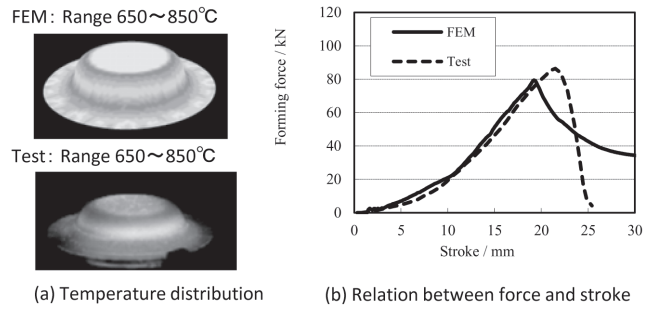


Fig. 24 Comparison of results between hot drawing test and simulation

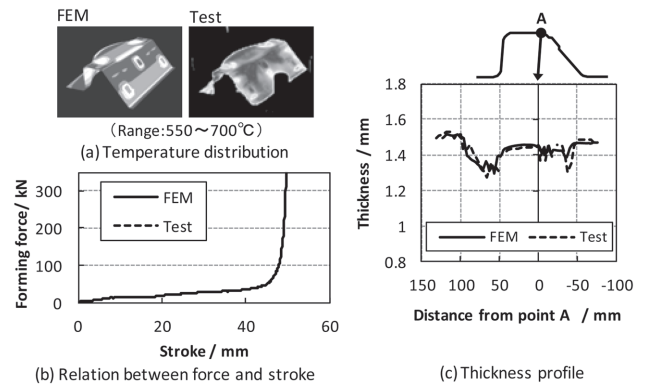


Fig. 25 Comparison of results between hot forming test and simulation

However, close observation of the temperature distribution after the test forming revealed that the die shape characteristics were more or less reflected in the temperature distribution. Therefore, we developed a method for correcting the temperature distribution in, e.g., curved sections that are subject to the influence of mesh size by referring to the geometrical shape of each individual part. The results of the calculations applying this method in hot drawing are shown in Fig. 24. While using an element size of about 2 mm, which is common in cold forming analysis, both the temperature distribution and forming force and the fracture during forming could be reproduced as a local element deformation. Fig. 25 illustrates the results obtained by applying this method in hot forming. We confirmed that the calculated temperature distribution, forming force, and thickness reduction agree well with the corresponding measured values.

3.4 Application of FEM simulation to actual parts

We applied the newly constructed condition correction technique in a hot forming simulation of an industrial part and compared the simulation results with test results. The part tested was a B-pillar model that was hot formed on a crank press at an operating speed of 30 spm (initial forming speed: 300 mm/s). Fig. 26 shows examples of comparison between the simulation results and the test results. Comparison of the thermal images shown in (a) confirmed that the calculated and measured temperature distributions almost agree. In the test, the wall portion was partly fractured. As shown in (b), the fractured part agreed with the part that exhibited a thickness reduction ratio of 30% or more in the analysis. Since other analyses have confirmed similar results, we consider it possible to predict fractures by studying thickness reduction.

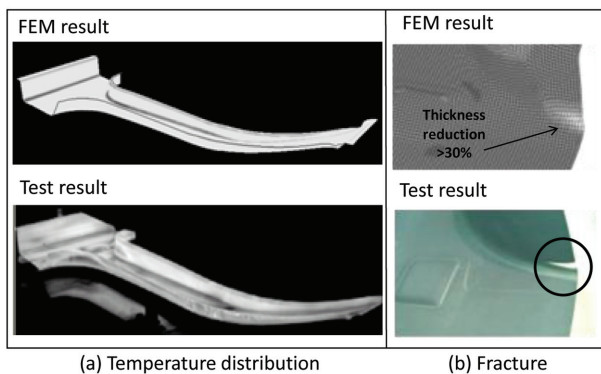


Fig. 26 Simulation results for hot stamping of a model part of industrial B-pillar

4. Conclusion

Here, we have described the basic press formability in hot stamping, the corrosion resistance of pressed parts, and forming analysis technology. In terms of press formability, we found that excellent shape fixability of steel sheet can be obtained because of the effect of its martensite transformation during quenching after forming. We also found an uneven temperature distribution as a result of contact between the steel sheet and the tool during forming and discovered that the resulting unevenness of material characteristics governs the forming limit. Furthermore, we found that aluminized steel sheet for hot stamping has an Al-Fe alloy layer with good corrosion resistance on the surface, that this layer retains its good corrosion resistance even if cracked during press forming, and that a phosphate crystal is deposited on the formed parts. As for the FEM simulation of forming, we accurately identified mechanical properties and friction and heat transfer coefficients under high temperatures, developed a heat transfer model reflecting the geometrical

shapes of parts, and thereby developed a new simulation technique applicable to actual automotive parts.

Hot stamping permits the manufacture of high-strength parts with good shape fixability. Using hot-stamping-coated steel sheet, it is also possible to obtain parts with good corrosion resistance. We hope that the basic knowledge relating to press forming and the forming analysis technique presented in this report will help expand the application of hot stamping and further reduce the weight of car bodies in the future.

References

- 1) Bano, X., Laurent, J. P.: Proc. of 39th Mechanical Working and Steel Processing Conf. Vol. XXXV, Indianapolis, 1998, p. 673
- 2) Suehiro, M., Maki, J., Kusumi, K., Ohgami, M., Miyakoshi, T.: Shinnittetsu Giho. (378), 15 (2003)
- 3) Ohgami, T., Takechi, H., Furuno, Y.: Journal of the Japan Society for Technology of Plasticity (J. JSTP). 28, 225 (1987)
- 4) Ohgami, T., Takechi, H., Furuno, Y.: J. JSTP. 28, 706 (1987)
- 5) Kusumi, K., Yamamoto, S., Takeshita, T., Nakamura, S., Abe, M., Suehiro, M.: CAMP-ISIJ. 18, 556 (2005)
- 6) Kusumi, K., Yamamoto, S., Takeshita, T., Abe, M.: Collection of Lecture Papers for 56th Joint Lecture Meeting of the Japan Society for Technology of Plasticity. 2005, p. 435
- 7) Yamanaka, S., Sakanoue, T., Yoshii, S., Inoue, T.: Materials. 48, 733 (1999)
- 8) Otsuka, T., Wakasu, Y., Inoue, T.: Collection of Lecture Papers for Academic Lecture Meeting of the Society of Materials Science, Japan. 52, 111 (2003)
- 9) Kusumi, K., Yamamoto, S.: Collection of Lecture Papers for 58th Joint Lecture Meeting of the Japan Society for Technology of Plasticity. 2007, p. 83
- 10) Kusumi, K., Yamamoto, S.: Collection of Lecture Papers for Spring 2010 Lecture Meeting of the Japan Society for Technology of Plasticity. 2010, p. 301
- 11) Maki, J. et al.: The 3rd Int. Conf. on Hot Sheet Metal Forming of High Performance Steel, Chs2 2011, 2011, p. 499
- 12) Dosdat, L. et al.: Steel Research Int. 82 (6), 726 (2011)
- 13) Okada, E. et al.: Surface Technology. 55 (11), 719 (2004)
- 14) Akira, Y. et al.: CIRP Annals. 58 (1), 247 (2009)



Kazuhisa KUSUMI
Manager
Research Planning Dept.
Steel Research Laboratories
20-1 Shintomi, Futtsu, Chiba 293-8511



Jun MAKI
Chief Researcher, Dr.
Yawata R&D Lab.



Naruhiko NOMURA
Senior Researcher
Forming Technologies R&D Center
Steel Research Laboratories